

Journal of Materials Chemistry C

Accepted Manuscript



This is an *Accepted Manuscript*, which has been through the Royal Society of Chemistry peer review process and has been accepted for publication.

Accepted Manuscripts are published online shortly after acceptance, before technical editing, formatting and proof reading. Using this free service, authors can make their results available to the community, in citable form, before we publish the edited article. We will replace this *Accepted Manuscript* with the edited and formatted *Advance Article* as soon as it is available.

You can find more information about *Accepted Manuscripts* in the [Information for Authors](#).

Please note that technical editing may introduce minor changes to the text and/or graphics, which may alter content. The journal's standard [Terms & Conditions](#) and the [Ethical guidelines](#) still apply. In no event shall the Royal Society of Chemistry be held responsible for any errors or omissions in this *Accepted Manuscript* or any consequences arising from the use of any information it contains.

Chemically Directed Self-Assembly of Perpendicularly Aligned Cylinders by Liquid Crystalline Block Copolymer

Cite this: DOI: 10.1039/x0xx00000x

Received 00th January 2012,

Accepted 00th January 2012

DOI: 10.1039/x0xx00000x

www.rsc.org/

N. Yamashita,^a S. Watanabe,^b K. Nagai,^a M. Komura,^a T. Iyoda,^{*,a, b} K. Aida,^c Y. Tada,^c and H. Yoshida^{*,c}

Chemical epitaxy with density multiplication process was applied to the perpendicularly oriented hexagonal cylinder nanostructure of liquid crystalline block copolymer (PEO-*b*-PMA(Az)) thin film through thermally induced microphase separation by using newly designed PMA(Az)₂₄ brush. The hexagonal lattice orientation with 1.9 tera-cylinders/inch² was laterally controlled for long-range-ordered direct self-assembly. Furthermore, the direct pattern-transfer of the assembled structure to an Au nanodot array was demonstrated by doping of H₂AuCl₄ selectively into the PEO cylindrical microdomains and then vacuum ultraviolet light irradiation to cause polymer etching and reduction of the Au ions.

1. Introduction

Photolithography has been powerful method widely for surface nanopatterning on various substrates in the recent progress of semiconductor industry and the smallest size achieved by the most advanced technique reaches about 15 nm in half-pitch. Toward the next-generation lithography with 10 nm or below¹, much attention has been drawn to self-assembled nanostructures of block copolymer thin film as an alternative technique. The periodic nanostructures such as body-centered cubic lattices of spheres, lamellae, gyroids, and hexagonally arranged cylinders^{2,3} are formed with dimensions between 5 to 100 nm through microphase separation. Especially, lamellae or cylindrical microdomains perpendicular to substrates can be readily applied as lithographic masks. However, actual use of the block copolymers has been still limited due to the difficulties in obtaining long-range lateral ordering and controlling the microdomain orientation.

To overcome this situation, graphoepitaxy⁴⁻⁸ and chemical epitaxy⁹ processes were developed to direct the self-assembly

and to place the microdomains on intended locations. The directed self-assembly (DSA) facilitates orientation-defined ordering and defect suppression. Nealey and coworkers demonstrated epitaxial assembly of perpendicularly oriented microdomains of poly(styrene-*b*-methacrylate) (PS-*b*-PMMA) on chemically pre-patterned templates with periodicity ranging from 20 to 50 nm fabricated by advanced lithographic techniques.⁹⁻¹⁴ Furthermore, their recent studies established a DSA process flow, which is compatible with semiconductor fabrication plants, and achieved minimum defect level required by the industry.¹⁵

Challenges still remain both in materials and processes of DSA to further minimize pattern dimensions, maintaining the perpendicular orientation of the microdomains in thin films. The minimum feature size of the assembled nanostructure is determined by its segregation energy, which is represented by the product of the Flory-Huggins interaction parameter (χ) and the total polymerization degree (N) of each segment composed by the block copolymer. The second important point is that perpendicular orientation of the microdomains in thin film

configuration is ensured by neutral tension of the segment to the film surface. PS-*b*-PMMA, one of the rare block copolymers to fulfill the neutral condition at thermal annealing temperature, has potential limitation on the minimum periodicity of the pattern down to ca. 20 nm in full pitch due to weak segregation force between PS and PMMA. Alternative types of block copolymers possessing higher χ parameters have been widely investigated to overcome this limitation,¹⁶⁻¹⁸ but in turn it is difficult to achieve perpendicularly oriented structures solely by applying a simple thermal annealing process. The polymer segments of the high- χ block copolymers have contrastive wettability to a substrate, so that the resulting lamella or cylinder is oriented parallel to the surface.¹⁹ Another strategy to adopt single layers of parallel cylinders or spheres have been taken in for DSA applying a simple thermal annealing process.

In order to satisfy both smaller feature sizes and perpendicular orientation, we propose to apply side-chain liquid crystalline (LC) block copolymers. Several researches have revealed the significant effects of LC ordering of the side-chains on the microphase separation due to homeotropic orientation of the liquid crystalline microdomains.²⁰⁻²³ Interaction between the LC side-chains dominates the interaction between the polymer blocks, and thus the LC ordering strongly influences the microphase separated structures of the LC block copolymers. PEO-*b*-PMA(Az), one of such block copolymers, consists of poly(ethylene oxide) (PEO) as a segment forming cylindrical microdomains, and poly(methacrylate) with azobenzene mesogens in the side chain (PMA(Az)) as a segment forming a matrix phase (Figure 1).²⁴⁻²⁸ In contrast to the conventional non-LC block copolymers, the LC azobenzene mesogen-mesogen interaction functions as an additional elastic energy term (F_{LC}) in the expression of total free energy (F) of the PEO-*b*-PMA(Az) thin film system. Total free energy of the system is given by the following equation.¹³

$$F = F_{\text{poly, poly}} + F_{\text{elastic}} + F_{\text{poly, air}} + F_{\text{poly, sub}} + F_{LC} \quad (1)$$

where $F_{\text{poly, poly}}$ is the interfacial energy between PEO and PMA(Az), F_{elastic} is the conformational entropy of the polymer chains, $F_{\text{poly, air}}$ is the interfacial energy between the polymer and the free air surface, and $F_{\text{poly, sub}}$ is the interfacial energy between the polymer and the substrate. The hydrophilic PEO and hydrophobic PMA(Az) segments are highly segregated, and F_{LC} further enhance the total segregation power between the segments. Actually, a periodicity as small as 7 nm in full pitch was achieved in the PEO hexagonal cylindrical microdomains in PEO₂₁-*b*-PMA(Az)₂₀.^{27, 28}

Another advantage is perpendicular orientation of the PEO hexagonal cylindrical microdomains to a substrate by just thermal annealing process, which is due to homeotropic anchoring of the Az mesogens to the air/free interface. The PEO cylindrical microdomains come down from the air surface towards the substrate surface during the cooling step of thermal annealing process.²⁴⁻²⁹ With these characteristics, PEO-*b*-PMA(Az) can form perpendicularly oriented cylinders with smaller feature size on various substrates, without applying

additional ingenuities such as pre-treatment of substrate surface, application of extra field such as an electric field, nor control of interfacial energy of the free surface.³⁰⁻⁴⁰

Herein, we applied chemical epitaxy method with density multiplication process to DSA of PEO-*b*-PMA(Az) and obtained orientation-controlled array of the PEO cylindrical microdomains, hexagonally in lateral and perpendicularly in axial directions, with periodicity below 10 nm half pitch. The chemical epitaxy of PEO-*b*-PMA(Az) was achieved by applying lithographically defined templates, whose surface was modified with newly synthesized PMA(Az)-OH brush. We also report a direct pattern-transfer of the assembled structure to orientation-defined gold nanodot array by selective doping of Au ions into the perpendicularly oriented cylindrical PEO domains with hydrophilic nature, followed by simultaneous reduction and block copolymer etching.

2. Experimental details

2.1. Materials

PMA(Az)₂₄-OH was newly synthesized as a LC brush layer for the LC block copolymer, PEO-*b*-PMA(Az), due to chemical matching between them, by atom transfer radical polymerization (ATRP). The number-averaged molecular weight, M_n , was determined to be 12 kg·mol⁻¹ and polydispersity index, M_w/M_n , was determined to be 1.2. Hydroxyl-terminated polystyrene PS₃₅-OH had $M_n = 3.7$ kg·mol⁻¹ and $M_w/M_n = 1.1$, which was commercially available from Polymer Source Inc., Canada. Amphiphilic LC diblock copolymer, PEO₁₁₄-*b*-PMA(Az)₂₄ (M_n : 5 kg·mol⁻¹ - 11.8 kg·mol⁻¹, $M_w/M_n = 1.1$, weight fraction of PMA(Az) $\phi_{\text{PMA(Az)}} = 0.72$), was synthesized by ATRP according to our previous report.^{24, 25} These chemical structures are shown in Figure 1. Details of the PMA(Az)₂₄-OH and PEO₁₁₄-*b*-PMA(Az)₂₄ synthesis are described in the supporting information and figures therein (at Figure S1 and section 2). The PEO₁₁₄-*b*-PMA(Az)₂₄ self-assembles PEO cylindrical microdomains in a PMA(Az) matrix. The (10) lattice spacing of hexagonally arranged PEO microdomains measured by small-angle X-ray scattering (SAXS) was 16.8 nm. The properties of PMA(Az)₂₄-OH, PS₃₅-OH, and PEO₁₁₄-*b*-PMA(Az)₂₄ are summarized in Table 1.

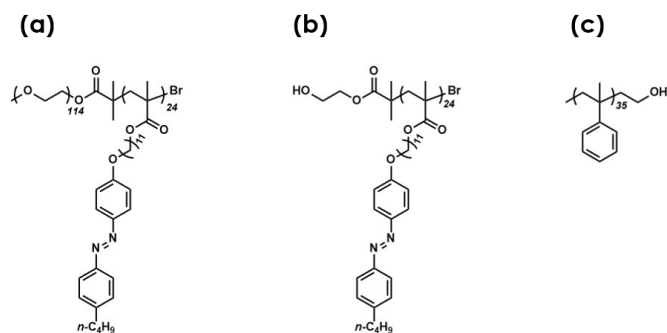


Fig. 1 Chemical structures of (a) PEO₁₁₄-*b*-PMA(Az)₂₄, (b) newly synthesized PMA(Az)₂₄-OH, and (c) commercially available PS₃₅-OH.

Table 1. Characterization of polymers used in this study.

Materials	M_n (kg/mol)	M_w/M_n	PEO weight fraction
PMA(Az) ₂₄ -OH	12	1.2	-
PS ₃₅ -OH	3.7	1.1	-
PEO ₁₁₄ - <i>b</i> -PMA(Az) ₂₄	16.8	1.1	0.28

2.2. Substrates

Before use, Si wafers were cleaned by immersion in piranha solution (7:3 mixture of concentrated sulfuric acid (H₂SO₄) and 30 wt% aqueous hydrogen peroxide (H₂O₂)) at 80 °C for 10 min, washed with deionized water, and dried by applying a nitrogen gas stream.

Chemically modified substrates were prepared by the process described below. The piranha-cleaned Si substrates were spin-coated with 1.0 wt% PMA(Az)₂₄-OH or PS₃₅-OH dissolved in toluene. The PMA(Az)₂₄-OH or PS₃₅-OH were grafted onto the Si substrates by annealing at 170 °C for 48 h under vacuum. After the thermal treatment, the substrates were rinsed twice with toluene to remove unreacted hydroxyl-terminated polymer chains. PMA(Az)₂₄-OH and PS₃₅-OH layers were formed on the Si substrates. The attachment of the hydroxyl-terminated polymers on the substrate was confirmed by X-ray photoelectron spectroscopy (XPS) (AXIS-HS, Shimadzu KRATOS Co.). A tapping mode atomic force microscope (AFM) (Dimension Icon, Veeco) measurement was carried out to characterize surface topology of the brush layers (see supporting information Figure S2). The thicknesses of the brush layers were measured by

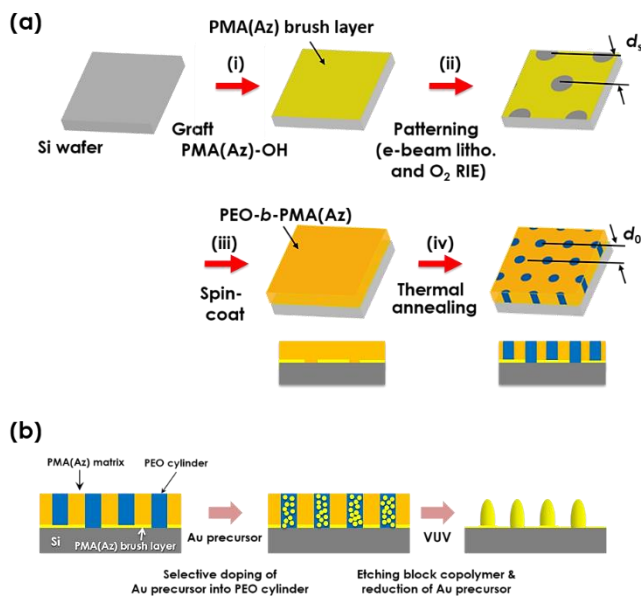


Fig. 2 (a) Schematic illustration of a chemical epitaxy process. (i) grafting of PMA(Az)₂₄-OH onto a Si wafer, (ii) patterning of PMA(Az)₂₄ brush layer by e-beam lithography, O₂ RIE (iii) PEO₁₁₄-*b*-PMA(Az)₂₄ coating, and (iv) thermal annealing at 140 °C for 2 h. (b) Schematic illustration of a fabrication process of an Au nanorod array templated by PEO microdomains of PEO-*b*-PMA(Az) self-assembled on the chemically patterned template of $d_s = 35$ nm with 4x density multiplication.

Table 2. Characteristics of the surfaces of bare, PS brush modified-, and PMA(Az) brush modified Si substrates.

Brushes	Thickness of brush layer (nm)	XPS C1s (CPS)	XPS N1s (CPS)	Contact angle (degree)
None	-	6.2×10^2	-	< 5
PS ₃₅ -OH	5	2.7×10^4	-	88
PMA(Az) ₂₄ -OH	4	8.6×10^3	5.2×10^2	83

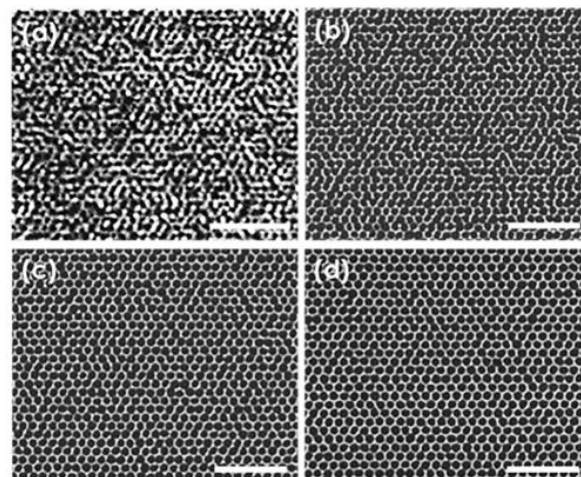


Fig. 3 SEM images of PMMA resist layers patterned by e-beam lithography. Lattice spacing d_s of hexagonally positioned circular holes patterned in the PMMA resist layers were (a) 29 nm, (b) 33 nm, (c) 35 nm and (d) 36 nm. All scale bars indicate 100 nm. Bright area shows PMMA resist, while dark circular areas are holes opened in the PMMA resist layers.

ellipsometry (ESM-4500, ULVAC). The characteristics of the PMA(Az) and the PS brush layers thus obtained are summarized in Table 2.

2.3. Chemical epitaxy

Chemical epitaxy of PEO-*b*-PMA(Az) was carried out following a process schematically illustrated in Figure 2 (a). Chemically patterned templates were prepared by patterning PMA(Az) brush layer deposited on Si substrate by electron beam (e-beam) lithography as shown in Figure 2 (a) (ii). Firstly, a PMMA layer was coated on the PMA(Az) brush surface as a positive e-beam resist. Secondly, a hexagonal array of circular holes was patterned in the PMMA layer by Vistec VB6 e-beam system operated at 100 kV, followed by wet development. A (10) lattice spacing of the hexagonally arranged holes (d_s) were designed to be 29, 33, 35 and 36 nm. The d_s values were varied around twice the (10) lattice spacing of PEO cylindrical microdomains self-assembled by PEO₁₁₄-*b*-PMA(Az)₂₄ on Si substrates (d_0). Thirdly, the PMA(Az) brush layer was patterned by oxygen reactive ion etching (O₂ RIE) using the patterned PMMA layer as a mask. The SEM images of the remaining PMMA resist layers after O₂ RIE process are presented in Figure 3. Finally, the PMMA resist layer was removed by dissolving in N-methylpyrrolidone and toluene solution.

In the next step, PEO₁₁₄-*b*-PMA(Az)₂₄ thin films were spin-coated on the patterned PMA(Az) brush surfaces from 1.5 wt % toluene solution (Figure 2 (a) (iii)). Unless otherwise stated, film thickness (t_f) of PEO₁₁₄-*b*-PMA(Az)₂₄ was 25 nm. The PEO₁₁₄-*b*-PMA(Az)₂₄ films were self-assembled by thermal annealing at 140 °C for 2 h and natural cooling to the room temperature under vacuum (Figure 2 (a) (iv)). Morphology of the self-assembled films thus obtained was observed by a field emission scanning electron microscope (SEM, S-4800 and SU-8020, Hitachi High-Technologies). The PEO microdomains were selectively stained by RuO₄ for improved contrast under the SEM measurements.

2.4. Direct pattern transfer of PEO cylindrical microdomains to Au nanodot

Au precursor was selectively doped into the PEO cylindrical microdomains of the PEO-*b*-PMA(Az) thin film self-assembled on the chemically patterned template by placing an aqueous solution of hydrogen tetrachloroaurate(III) tetrahydrate (HAuCl₄·4H₂O) (0.5 M) on the PEO-*b*-PMA(Az) surface for 2 h at room temperature. After doping, the sample surface was rinsed with ethanol to remove excess gold ions remaining on the PEO-*b*-PMA(Az) surface and dried by applying a stream of nitrogen gas. The samples were then irradiated by vacuum ultraviolet (VUV) for 30 min with a Xe excimer lamp ($\lambda = 172$ nm, 10 mW·cm⁻¹, 30 Pa, UER20H-172A, USHIO Inc.) in order to reduce Au³⁺ ions in PEO cylinders to zero valence Au⁰ as seen in Figure 2 (b). By this procedure, metal nanodots were formed and block copolymer thin film was removed, simultaneously. The structure of Au nanodot arrays was observed by SEM (SU-8020, Hitachi High-Technologies).

3. Results and discussion

3.1. Morphology of PEO₁₁₄-*b*-PMA(Az)₂₄ thin film on Si wafers

Figure 4 shows a top-view SEM image of the PEO₁₁₄-*b*-PMA(Az)₂₄ thin film self-assembled on Si wafer by thermal annealing, its 2-dimensional fast Fourier Transform (2D-FFT) image, and a cross-sectional SEM image of the thin film. Thickness of the PEO₁₁₄-*b*-PMA(Az)₂₄ thin film was 50 nm for this observation. As seen in Figure 4 (a), the PEO microdomains, which appear with bright contrast under SEM, formed hexagonal packed arrangement. Perpendicular orientation of the PEO cylinders in axial direction against the substrate was confirmed by the cross-sectional image (Figure 4 (c)). The (10) lattice spacing of PEO cylindrical microdomains assembled on the Si surface (d_0) was determined to be 17.5 nm from the positions of the peaks in the 2D-FFT image (Figure 4 (b)). The d_0 was slightly larger than that of the bulk determined by a small angle X-ray scattering measurement, i.e. 16.8 nm. As can be seen in Figure 4 (a), assembly of PEO-*b*-PMA(Az) has superior long-range order forming large ordered grains, which might be due to its large segregation force and LC ordering. However, grain boundaries still exist and orientation of the lattice gradually alters with distance as detected in the 2D-FFT image as isotropic halos coexisting with spots. In order to design and arrange the

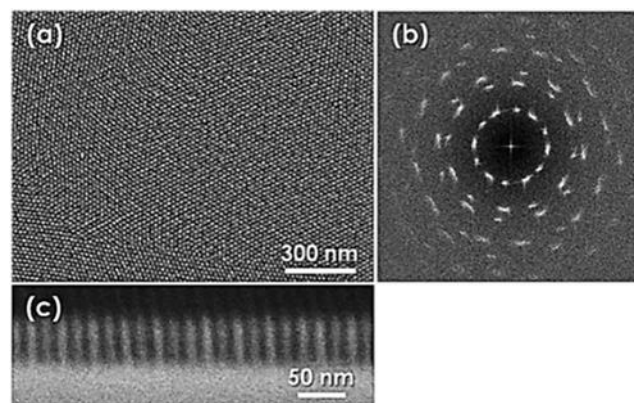


Fig. 4 (a) A SEM image of PEO₁₁₄-*b*-PMA(Az)₂₄ thin film self-assembled on a Si wafer and (b) its 2D-FFT image. (c) Cross-sectional SEM image of the PEO₁₁₄-*b*-PMA(Az)₂₄ thin film self-assembled on a Si wafer. PEO microdomains of the sample were selectively stained with RuO₄ to obtain contrast under SEM, which appear brighter compared to the unstained PMA(Az) matrix. Film thickness was 50 nm.

cylindrical microdomains in a controlled orientation-defined structure, we introduced directed self-assembly of PEO-*b*-PMA(Az) applying chemical epitaxy process.

3.2. Evaluation of PMA(Az) brush layer on Si wafer

Chemical epitaxy of block copolymer thin films utilizes pre-patterned templates with surface energy contrast to direct the location of the self-assembled microdomains.^{2, 11, 12} For PS-*b*-PMMA system, there is an established method to modify the surface energy by forming PS-*ran*-PMMA brush layer on the substrate surface.⁴¹ In this study, we first tried to develop a brush material, which is suitable to achieve chemical epitaxy of PEO-*b*-PMA(Az).

PEO-*b*-PMA(Az) is composed of hydrophilic PEO and hydrophobic PMA(Az). Therefore, chemical templates composed of hydrophilic and hydrophobic surfaces might be applicable for the directed self-assembly of PEO-*b*-PMA(Az). As oxidized Si surface is hydrophilic, we investigated two kinds of polymer brushes to modify the Si surface to hydrophobic nature. One of the brushes was composed of PS, which has been widely used for the chemical modification, and the other was composed of PMA(Az), which has the same chemical structure as one of the components of PEO-*b*-PMA(Az). Hereinafter referred to as PMA(Az) brush and PS brush layers, respectively.

The PS and PMA(Az) brush layers were deposited on Si substrates by grafting hydroxyl terminated polymers, i.e. PS-OH and newly synthesized PMA(Az)-OH, respectively. Formation of the brush layers was confirmed by X-ray photoelectron spectroscopy (XPS) measurements (Table 2). The intensity of C 1s peak at 284 eV detected from the PS and PMA(Az) brush surfaces increased more than one order of magnitude compared to that detected from the bare Si substrates. Note the C 1s signal detected from the bare Si substrate might be due to organic surface contamination. A N 1s peak at 399 eV, which corresponds to the N=N bond of the azobenzene mesogens, was only detected from the surface with PMA(Az) brush layer. These

results confirm the existence of PS and PMA(Az) brushes on the Si wafers. AFM measurements of the substrate with brush layers also indicated the existence of brushes on the Si substrates (shown in Figure S2).

In order to understand the wettability of the brush surfaces, we measured contact angle of the water against three kinds of substrates; bare Si substrate oxidized by O₂ RIE treatment, Si substrate with PS brush, and Si substrate with PMA(Az) brush. As listed in Table 2, oxidized Si surface was completely hydrophilic with contact angle less than 5°. On the other hand, the PS brush and the PMA(Az) brush surfaces exhibited similar contact angle around 85°, which confirms that surfaces modified with these brushes were significantly hydrophobic.

As a next step, we studied the behavior of PEO-*b*-PMA(Az) thin film on the brush surfaces. The thin films of PEO₁₁₄-*b*-PMA(Az)₂₄ were coated on the PS brush (Figure 5 (c) and (d)) and the PMA(Az) brush surfaces (Figure 5 (a) and (b)), and subsequently self-assembled by thermal annealing. A PEO₁₁₄-*b*-PMA(Az)₂₄ block copolymer thin film was formed uniformly on the PMA(Az) brush surface (Figure 5 (a)), while partially dewetted from the PS brush surface (Figure 5 (c)). However, microscopically, hexagonal arrays of perpendicularly oriented PEO cylinders were assembled in the PEO-*b*-PMA(Az) film on the both surfaces, as can be clearly seen by the SEM images presented in Figures 5 (b) and (d). These results imply that the chemical composition of the brush layer had no discernible impact on the axial orientation of the cylindrical PEO microdomains, in spite of the significant difference in the wetting behavior of PEO-*b*-PMA(Az). For conventional non-LC block copolymers, including PS-*b*-PMMA, substrate surface have to be neutralized to orient the microdomains in the direction perpendicular to the substrate, which generally requires carefully tuning of the brush composition.⁴² This is not the case for PEO-

b-PMA(Az). As mentioned in the introduction section, the PEO microdomains in PEO-*b*-PMA(Az) thin film orient perpendicular against its free surface by homeotropic alignment of the LC mesogens in the matrix phase and grow down toward the substrate. Therefore, surface chemistry of the substrate does not influence the orientation of the PEO cylindrical microdomains.³⁷ This characteristic is especially attractive for the chemical epitaxy with density multiplication, which requires orienting microdomains perpendicularly on the brush surface at the location in between the chemical guiding marks.

To further understand the nature of the brush layers, number density of the polymer chains attached to the Si substrate (σ) was estimated using equation (2)^{43,44}

$$\sigma = \rho h N_A / M_n \quad (2)$$

where N_A represents the Avogadro's number, M_n is the number-average molecular weight of the polymer chain composing the brush layer, and h and ρ are the mean height and the mass density of the brush layer, respectively. For the PMA(Az) brush layer with $M_n = 12 \text{ kg}\cdot\text{mol}^{-1}$, which was employed in this study, h was measured to be 4 nm by ellipsometry, while the bulk value of 1.1 g·cm⁻³ was used for ρ on the assumption of little difference following previously reported papers.^{43,44} From these values, σ was estimated to be 0.22 nm⁻². The PMA(Az) chains form much stretched conformation than that of non-LC type polymers due to the existence of azobenzene mesogens in their side chains. Therefore, the PMA(Az) chains are expected to be spread on the substrate, while non-LC type block copolymer chains are normally expected to form mushroom type of the conformation. In spite of its lower σ , the PMA(Az) brush exhibited characteristics suitable for chemical epitaxy of PEO-*b*-PMA(Az) system. Its hydrophobicity can create significant chemical contrast against the oxidized Si surface and its surface can be coated uniformly with thin film of PEO-*b*-PMA(Az) without dewetting behavior. Therefore, we conclude that the newly synthesized PMA(Az) brush would be suitable to use for the chemical epitaxy of PEO-*b*-PMA(Az).

3.3. Directed self-assembly of PEO₁₁₄-*b*-PMA(Az)₂₄ with density multiplication

Chemical epitaxy of PEO₁₁₄-*b*-PMA(Az)₂₄ was studied applying patterned PMA(Az) brush layer as a chemical template followed by the process illustrated in Figure 6. As schematically illustrated in Figure 2 (ii), the chemical templates composed of the PMA(Az) brush surface with hexagonal array of circular openings with oxidized Si surfaces were fabricated by e-beam lithography. The (10) lattice spacing of the circular a with the oxidized Si surface, d_s , was designed according to the well-established relation of $d_s = n \times d_0$, where n should be an integer number for ideal density multiplication with a factor of n^2 .^{11,12} In this study, we varied n from 1.7 to 2.1 to investigate the effect of lattice spacing mismatch between the patterned template and the self-assemble block copolymer. Since the (10) lattice spacing of the PEO₁₁₄-*b*-PMA(Az)₂₄ assembled on Si wafer was $d_0 = 17.5 \text{ nm}$, four types of chemical patterns were fabricated with $d_s = 29$

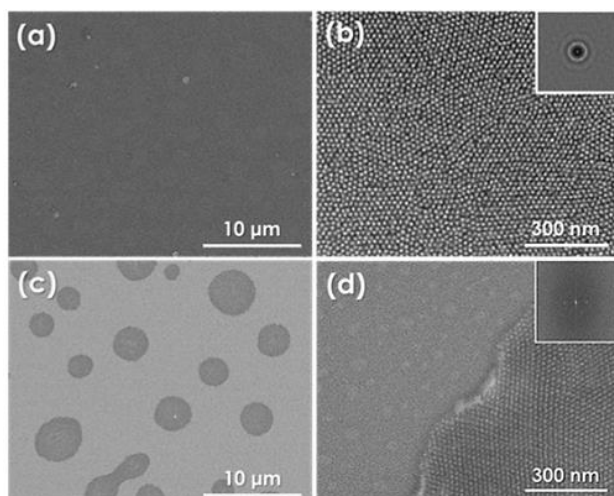


Fig. 5 SEM images of PEO₁₁₄-*b*-PMA(Az)₂₄ thin films on PMA(Az) brush layer ((a), (b)) and on PS brush layer ((c), (d)). Images (a) and (c) were observed under lower magnification, while images (b) and (d) were taken under higher magnification. PEO microdomains of the sample were selectively stained with RuO₄ to obtain contrast under SEM. Therefore, PEO domains appear brighter than PMA(Az) matrix in high magnification images ((c) and (d)).

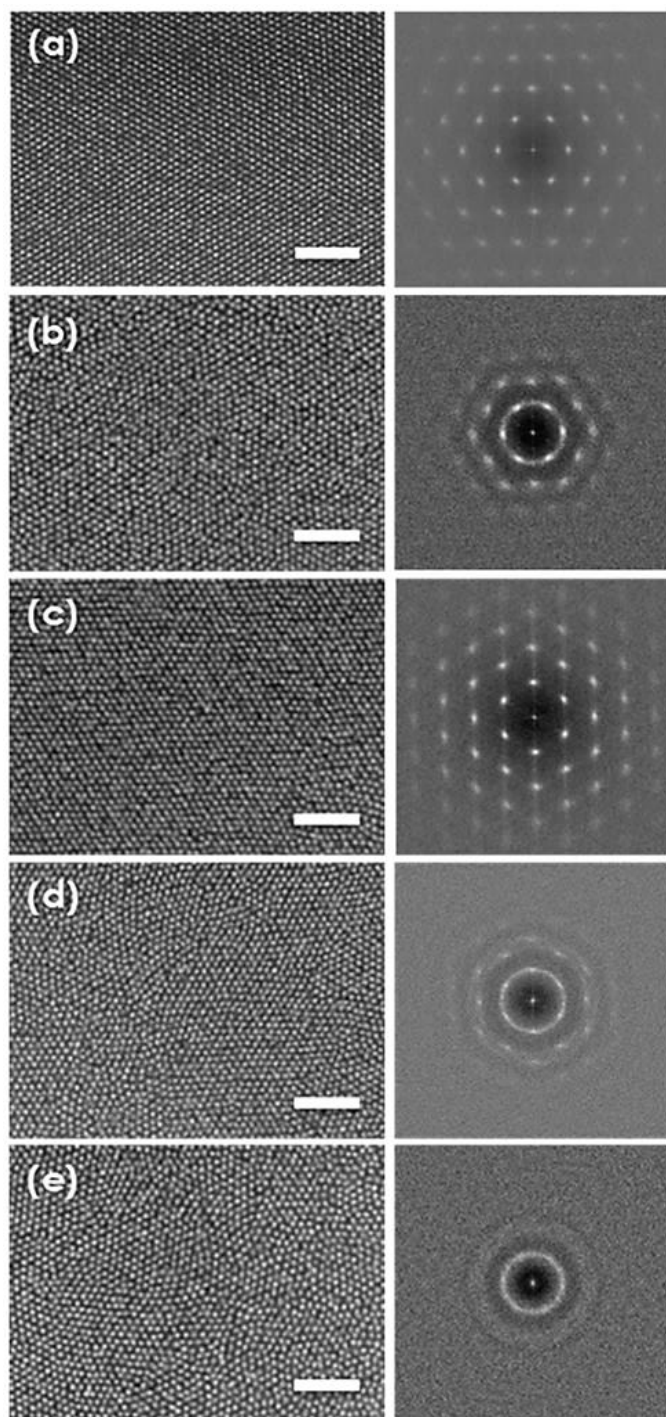


Fig. 6 SEM images and corresponding 2D-FFT images of the PEO₁₁₄-*b*-PMA(Az)₂₄ thin films assembled on the chemically patterned templates with lattice spacing of (a) $d_s = 29$ nm, (b) $d_s = 33$ nm, (c) $d_s = 35$ nm, (d) $d_s = 36$ nm and (e) on the un-patterned region of the template. The templates were fabricated by patterning PMA(Az) brush layer by e-beam lithography. All scale bars indicate 200 nm. PEO microdomains of the sample were selectively stained with RuO₄ to obtain contrast under SEM, which appear brighter compared to the unstained PMA(Az) matrix.

nm ($n = 1.7$), $d_s = 33$ nm ($n = 1.9$), $d_s = 35$ nm ($n = 2.0$) and $d_s = 36$ nm ($n = 2.1$). The PEO₁₁₄-*b*-PMA(Az)₂₄ thin films were uniformly coated and self-assembled by thermal annealing on the

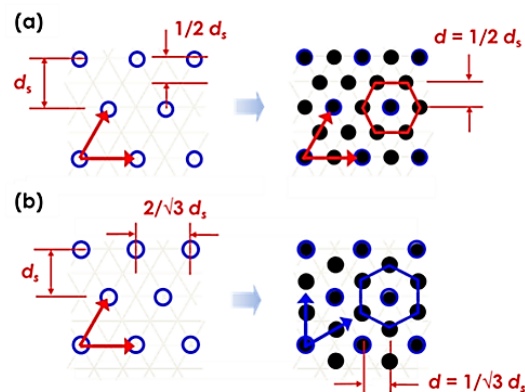


Fig. 7 Schematic illustrations demonstrating pattern interpolation manners for (a) 3 \times and (b) 4 \times density multiplication. Black filled circles (●) show hexagonal lattice points formed by the PEO cylindrical microdomains, and blue open circles (○) indicate the lattice of the underlying chemical template.

templates with different d_s . Dewetting behavior was not observed. Top-view structure of PEO₁₁₄-*b*-PMA(Az)₂₄ thin films on the patterned templates, as well as on the un-patterned PMA(Az) brush layer, were captured by SEM and obtained images are summarized in Figure 6.

First, as shown in Figure 6 (c), PEO₁₁₄-*b*-PMA(Az)₂₄ assembled almost a single hexagonal lattice of perpendicularly oriented cylindrical PEO microdomains on the chemical template with $d_s = 35$ nm ($n = 2.0$). The corresponding 2D-FFT image exhibited hexagonal spots with 4 orders of peaks. The lateral orientation of the hexagonal lattice of the PEO microdomains agreed with that of the underlying chemical template. Analysis of the peak positions in the 2D-FFT image gave an average (10) lattice spacing of the PEO microdomains (d) of 17.5 nm, which was equal to d_0 , and was half of the lattice spacing of the template d_s . From these results, we concluded that the PEO cylindrical microdomains were registered on the template as illustrated in Figure 7 (a). The PEO microdomains should be located on and in between the chemical patterns, multiplying the density of the chemical template by a factor of 4. The areal density of the hexagonal lattice achieved was 1.9 tera-rods/inch². Most importantly, we emphasized that ultrahigh density lattice of perpendicularly oriented cylindrical microdomains were obtained with controlled lateral orientation.

Figure 6 (a) shows the morphology of PEO₁₁₄-*b*-PMA(Az)₂₄ thin film on the chemical template with $d_s = 29$ nm ($n = 1.7 \approx \sqrt{3}$). Although the PMMA resist employed to prepare the chemical template consisted considerable amount of defects (see Figure 3 (a) in the experimental section), the PEO microdomains formed a single hexagonal lattice with less-defects. The corresponding 2D-FFT image exhibited hexagonal spots with 4 orders of peaks. The lattice spacing of the self-assembled lattice determined from the 2D-FFT image was $d = 17.0$ nm, which was closed to $1/\sqrt{3}$ of d_s . In addition, the orientation of the self-assembled lattice was 30° rotated compared to that of the underlying template (compare the orientation of the lattice of the template presented in Figure

3 (a) and that of the self-assembled PEO cylindrical microdomain in Figure 6 (a)). These results imply that the PEO cylindrical microdomains were arranged on the template with a manner illustrated in Figure 7 (b) and, as a result, the density of the template was multiplied by a factor of 3. On the templates with $d_s = 33$ nm ($n = 1.9$) and $d_s = 36$ nm ($n = 2.1$), SEM observations revealed that the cylindrical PEO microdomains were partially registered on the template forming distorted lattice. For $d_s = 33$ nm, as presented in Figure 6 (b), 2D-FFT pattern of the SEM image exhibited hexagonal spots coexisting with weak halo peaks. The orientation of hexagonal spots was found to be same as that obtained for $d_s = 29$ nm. An average lattice spacing determined from spot positions was $d = 18.6$ nm, which corresponded roughly to $1/\sqrt{3}$ of d_s . These results suggest that the PEO microdomains were arranged partially on the template with the same but with much imperfect manner compared to that for $d_s = 29$ nm, multiplying the density of the template with a factor of 3. For $d_s = 36$ nm, the 2D-FFT image showed halo peaks with weak hexagonal spots as presented in Figure 6 (d). The orientation of the hexagonal spots was same as that observed in the 2D-FFT pattern for $d_s = 35$ nm. Position of the spots corresponded to $d = 18.1$ nm, which was half the value of d_s . These results suggest that the PEO microdomains were directed to form the lattice on the chemical template obeying the manner for the 4x density multiplication, but resulted in the distorted arrangement.

By inspection of the morphologies of PEO₁₁₄-*b*-PMA(Az)₂₄ thin films self-assembled on the chemical templates with d_s of 29, 33, 35, and 36 nm, only templates with $d_s = 29$ and 35 nm were found to be effective to obtain orientation- defined lattice with density multiplication. These findings suggest that precise control of the lattice dimensions of the chemical template is necessary to achieve epitaxial arrangement of the PEO cylindrical domains. In the case for 3x density multiplication, PEO microdomains were registered on the template with $d_s = 29$ nm resulting in the orientation-defined single lattice with $d = 17.0$ nm, while the lattice obtained on the template with $d_s = 33$ nm was partially distorted with $d = 18.6$ nm. As natural domain spacing of the PEO₁₁₄-*b*-PMA(Az)₂₄ was $d_0 = 17.5$ nm, it can be roughly estimated that the domain spacing was compressed about 3 % for the former case and extended about 6 % for the latter case. Similarly, in the case for 4x density multiplication, the PEO microdomains formed defined single lattice with $d = 17.5$ nm on the template with $d_s = 35$ nm, while the lattice obtained on the template with $d_s = 36$ nm was considerably distorted with $d = 18.1$ nm (103 % of d_0). These consideration may imply that domain spacing of PEO-*b*-PMA(Az) can be extended or compressed about a few percentage by the chemical template. The natural conformation of PMA(Az) segments of PEO-*b*-PMA(Az) are stretched with low flexibility, which are confined in smectic layer at the liquid crystalline state. Therefore, stretching or compressing of the main chains is expected to be energetically unfavored. However, in spite of these limitation, the current experimental results suggest that there are some flexibility in the domain spacing of PEO-*b*-PMA(Az) to register their microdomains on the chemical pattern of the template.

Nevertheless, the tolerance of the mismatch in lattice constant between the template and the block copolymer for PEO-*b*-PMA(Az) is smaller than that of the non-LC block copolymer. For example, Tada et al. observed that PS-*b*-PMMA can be stretched about 8 % to form single lattice by chemical epitaxy with 4x density multiplication.¹²

In addition to these experiments, voronoi analysis which is commonly used to characterize its region boundary was performed to calculate defect densities of the PEO cylindrical microdomains on the each substrate followed by procedure using free software of Image J as described in elsewhere.⁴⁵ The analysis was carried out for totally five nanopatterns on four different chemically patterned templates ($d_s = 29, 33, 25,$ and 36 nm) and non-patterned template. In case of the successfully demonstrated directed-self-assembly of the PEO cylindrical microdomains by the chemically patterned templates with $d_s = 29$ nm and 35 nm, there were few defects on the PEO cylindrical microdomains arrangement as shown in Figure S3 and Table S1 compared with that of the PEO microdomains without chemically patterned template. Moreover, the PEO cylindrical microdomains arrangement on the chemically patterned templates with $d_s = 33$ nm and 36 nm had quite larger amount of defects as compared to that on the templates with $d_s = 29$ nm, 33 nm, and even without chemically patterned template.

As mentioned in the introduction section, the orientation of the PEO cylindrical microdomain in the thin film was dominated by the LC homeotropic alignment to form perpendicular orientation. The PEO microdomains are known to come down from the free air interface to the substrate.²⁹ On the other hand, current study revealed that the lateral placement of the PEO cylindrical microdomains is predominated by the chemically patterned templates. In other words, in the chemical epitaxy process with PEO-*b*-PMA(Az), control of lateral placement and axial orientation of the PEO cylinders can be decoupled to a certain degree, the former controlled by the template surface and the latter by the free surface. These characteristic allow us to achieve chemical epitaxy of microdomains with perpendicular orientation against the substrate with density multiplication without utilizing neutralization of the brush layer.

3.4. Direct pattern-transfer of PEO cylindrical microdomains self-assembled on the chemical template to a single orientation-defined Au nanodot array

For the actual use in the applications, it is indispensable to transfer the patterns of the block copolymer thin film to the useful materials. We tried to transfer the hexagonal PEO microdomains assembled on a chemically patterned template to an Au nanodot array by applying template method reported previously.^{30, 35, 40} PEO is one of the well-known ion-conductive host materials. The template method employs the PEO cylindrical microdomains assembled by PEO-*b*-PMA(Az) as nano-sized ion reactors, into which Au precursors are selectively penetrated and are reduced to form Au nanodots.^{35, 40} Note, in our process, PEO chains were not removed / etched from the cylindrical microdomains to create nano-holes to transfer the

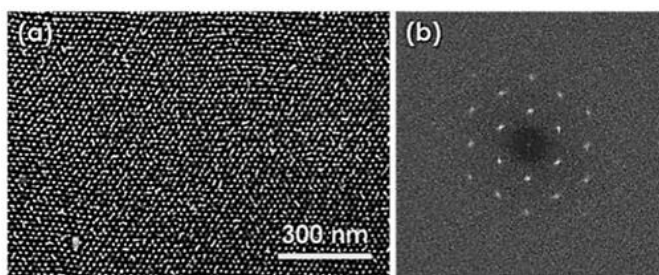


Fig. 8 (a) A SEM image of Au nanorod array templated by PEO cylindrical microdomains of PEO₁₁₄-*b*-PMA(Az)₂₄ self-assembled on the chemically patterned template of $d_s = 35$ nm with 4x density multiplication. The (10) lattice spacing was 17.5 nm, and (b) its corresponding 2D-FFT image.

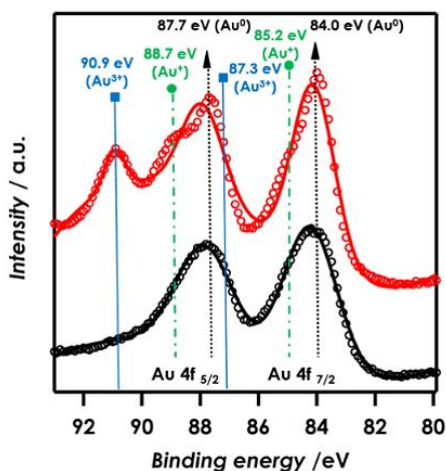


Fig. 9 XPS spectra of Au-doped PEO₁₁₄-*b*-PMA(Az)₂₄ thin film (black) and Au nanorod array after removal of the block copolymer thin film (red) in the binding energy region of Au 4f. Open circles are measured results and solid lines show their Gaussian fit.

pattern to gold nanodots as in the case for most of the pattern transfer processes.

The PEO cylindrical microdomains with $d = 17.5$ nm self-assembled by 4x density multiplication process on the chemically patterned template with $d_s = 35$ nm were transferred to Au nanodots following the process schematically illustrated in Figure 2 (b). First, the Au precursor was selectively doped into the PEO cylindrical microdomains. Selective doping was driven by the coordination of Au³⁺ ions to un-paired electrons on the oxygen atoms of PEO segments. The Au³⁺ ions inside the PEO cylindrical microdomains were then reduced to zero valence, and the block copolymer was etched simultaneously by the VUV irradiation for 30 min following the process reported previously.⁴⁰

Formation of the nanodot structure was confirmed by SEM observation presented in Figure 8 (a). A 2D-FFT image of the SEM image (Figure 8 (b)) exhibited hexagonal spots clearly showing that the Au nanodots were arranged in a single orientation-defined hexagonal lattice. The lateral orientation of the lattice and its lattice spacing determined from the peak positions of the 2D-FFT image were identical to those of the self-assembled PEO₁₁₄-*b*-PMA(Az)₂₄. From these findings, we

concluded that the PEO cylindrical microdomains were successfully transferred to the Au nanodots maintaining their arrangement defined by the chemical template.

The obtained sample with nanodots was analyzed by XPS to conform its composition. Figure 9 shows Au 4f XPS spectra of Au-doped PEO₁₁₄-*b*-PMA(Az)₂₄ thin film (black) and Au nanodot array after VUV irradiation (red). In the spectra of Au-doped PEO₁₁₄-*b*-PMA(Az)₂₄, two peaks were detected at 84.2 and 88.0 eV, which can be assigned as Au 4f_{7/2} and 4f_{5/2} relating to zero valence Au⁰, respectively. The Au precursor residue was still remained on the block copolymer thin film after rinsing with ethanol, so that zero valence Au⁰ was only detected by XPS measurement. In contrast, different Au valence states (Au³⁺, Au⁺, and zero valence Au⁰) were observed in the sample after VUV treatment. New peaks emerged at 85.2 eV, and 87.3, 88.7, and 90.9 eV, which can be assigned as Au 4f_{7/2} and 4f_{5/2}, respectively. These peaks can be attributed to Au⁺ and Au³⁺.^{40, 46, 47} These results reveal that Au ions penetrated inside the PEO cylindrical microdomains in the block copolymer thin film were partially reacted by the VUV irradiation intricately, and suggest that zero valence Au⁰ was formed simultaneously during the polymer etching process by the VUV treatment.

To study the uniformity of the process, SEM observations were performed at five discrete positions inside the patterned area of the chemical template, namely at the regions closed to the four edges and the center of the patterned area of 50×50 μm². As for the comparison, SEM observation was also conducted at the position outside the patterned region. The SEM images obtained are presented with their 2D-FFT images in Figures 10 (a) to (f), with the low magnification SEM image showing locations of the observations (Figure 10 (g)). The 2D-FFT patterns of the SEM images observed inside the patterned area were identical with hexagonal spots at same azimuth (Figures 10 (a) ~ (e)). On the other hand, the 2D-FFT image of the micrograph observed outside the patterned area revealed a halo peak, which indicated that Au nanodots are arranged in the non-orientation-defined distorted lattice (Figure 10 (f)). These results strongly suggest that the Au nanodots were arranged in a single lattice extending the whole patterned area.

Finally, we would like to note that, in this study, size of the patterned area was limited to 50×50 μm², mainly because of the limitation in the e-beam lithography to fabricate the chemical template. Therefore, the process can be extended to macroscopic size required for actual applications, by applying large scale photolithographic processes to fabricate the patterned templates. Moreover, the developed pattern-transfer process can be applied to various metals and metal oxides, as we have reported before.^{30-35, 38-40}

4. Conclusions

In this study we have demonstrated the fabrication of laterally orientation-defined lattice of perpendicularly oriented cylindrical microdomains in axial direction, applying chemical epitaxy of LC block copolymer, PEO-*b*-PMA(Az). The assembled structure was further transferred to gold nanodot array.

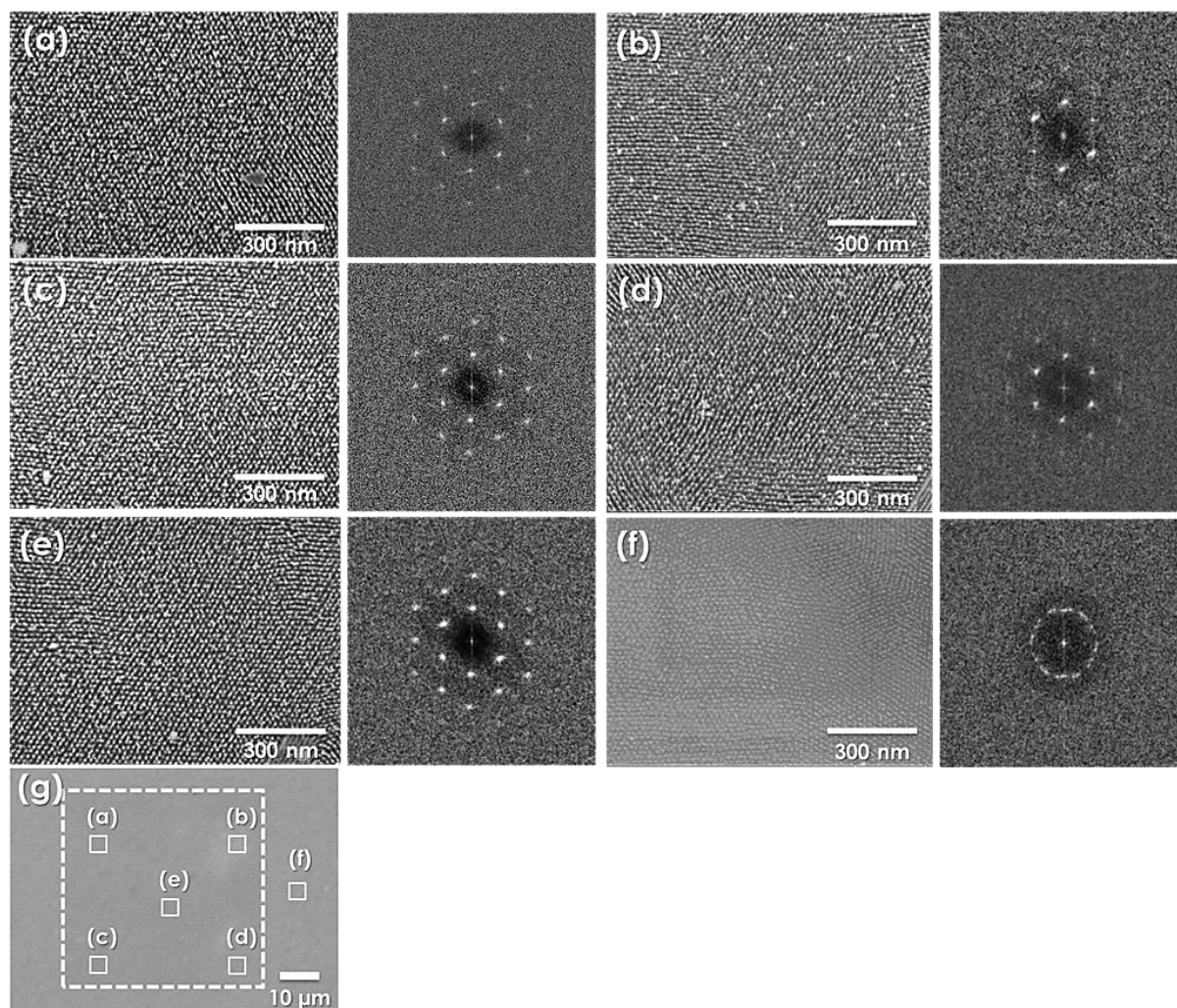


Fig. 10 SEM images of Au nanorod arrays observed at five discrete areas selected from the chemically patterned area of the template ((a) to (e)), and at the area outside the chemical pattern (f). The insets are 2D-FFT images corresponding to these SEM images. The SEM images were taken at the areas shown in a low magnification SEM image (g) over viewing whole chemically patterned region of the template.

The developed process is based on the unique combination of the polymers composing the block copolymer, i.e. hydrophilic PEO and hydrophobic PMA(Az) with liquid crystalline side groups.

First, we have demonstrated that the chemical epitaxy of PEO-*b*-PMA(Az) can be achieved by utilizing the chemical template prepared by patterning the newly synthesized PMA(Az) brush layer with e-beam lithography. A laterally orientation-defined lattice of perpendicularly oriented cylindrical PEO microdomains with areal density of 1.9 tera-rods/inch² was achieved by multiplying the density of the template by a factor of 4. The key factor for the successful assembly was to utilize LC block copolymer with strong segregation to obtain small feature size and to control the axial orientation of the cylindrical domains as well as their lateral placement. The former was achieved by the strong segregation between PEO and PMA(Az), which was further enhanced by the LC interaction in the PMA(Az) side chain. The latter, which is generally difficult to achieve by use of conventional high- χ block copolymers, was

realized by homeotropic alignment of the LC mesogens against the block copolymer film surface. In other words, by introducing LC moiety, we have shown the possibility to decouple the control of lateral placement and axial orientation of the microdomains, i.e. the former to be directed by the chemical template and the latter to be controlled by the film surface.

In the next step, we showed direct pattern-transfer of the assembled structure to an orientation-defined Au nanodot array. The pattern transfer was realized by selective doping of Au ion into the hydrophilic PEO microdomains, not removed to be nanoholes, which is another advantage in the PEO-*b*-PMA(Az)-based template processes. It might be important to emphasize that dense hydrophobic matrix composed of PMA(Az) with side chains forming smectic phase enhanced the selectivity of ion doping process. Although area of the Au nanodot array obtained in this study was limited to 50×50 μm², the process can be readily expanded to macroscopic size for industrial use by applying large scale lithographic tools. Furthermore, the selective doping process can be applicable to various materials (*e.g.* metals, metal

oxides, polymer, semiconductor, ion liquids) instead of Au. Therefore, the developed process, which combines nanolithography, self-assembly, and selective ion doping, with full utilization of LC interaction, provides a promising fabrication method for extension of lithographic capabilities to smaller dimensions below 10 nm.

Acknowledgements

We gratefully thank Drs. Lei Wang, Elizabeth Dobisz, and Ricardo Ruiz, HGST, a Western Digital Company, for their kind support in the e-beam lithography. This work was supported by a Grant-in-Aid for Scientific Research from the Japan Society for the Promotion of Science (No. 18101005). In addition, N.Y. was supported by the Global COE program (No. 19877718) at the Tokyo Institute of Technology.

Notes and references

^a Division of Integrated Molecular Engineering, Chemical Resources Laboratory, Tokyo Institute of Technology, 4259-R1-25, Suzukakedai, Yokohama-shi, Kanagawa, 226-8503, Japan.

^b Iyoda Supra-integrated Material Project (iSIM), ERATO, Japan Science and Technology Agency (JST), Chiyoda-ku, Tokyo, 4-5-3, Japan.

^c Hitachi Research Laboratory, Hitachi Ltd., Hitachi, Ibaraki, 319-1292, Japan.

Present Addresses

^a(M. K.) Department of Electrical and Electronics Engineering, Numazu National College of Technology, 3600 Ooka, Numazu, Shizuoka, 410-8501, Japan.

Notes

The authors declare no competing financial interest.

† Electronic Supplementary Information (ESI) available: [Additional characterization of PEO₁₁₄-*b*-PMA(Az)₂₄ block copolymer and PMA(Az)₂₄-OH, and AFM images of PMA(Az)₂₄-OH brush layer on Si wafer, and voronoi characterization.]. See DOI: 10.1039/b000000x/

- M. P. Stoykovich and P. F. Nealey, *Materials Today*, 2006, **9**, 20.
- S. O. Kim, H. H. Solak, M. P. Stoykovich, N. J. Ferrier, J. J. dePablo and P. F. Nealey, *Nature*, 2003, **424**, 411.
- C. T. Black, K. W. Guarini, K. R. Milkove, S. M. Baker, T. P. Russell and M. T. Tuominen, M. T. *Appl. Phys. Lett.*, 2001, **79**, 409.
- R. A. Segalman, H. Yokoyama and E. J. Kramer, E. J. *Adv. Mater.*, 2001, **13**, 1152.
- D. Sundrani and S. J. Sibener, *Macromolecules*, 2002, **35**, 8531.
- S. G. Xiao, X. M. Yang, E. W. Edwards, Y. H. La and P. F. Nealey, *Nanotechnology*, 2005, **16**, S324.
- F. Chen, S. Asakawa, T. Inoue, M. Takenaka, H. Hasegawa and H. Yoshida, *Macromol. Rapid Commun.*, 2007, **28**, 2137.
- L. Rockford, Y. Liu, P. Mansky, T. P. Russell, M. Yoon and S. G. J. Mochrie, *Phys. Rev. Lett.*, 1999, **82**, 2602.
- E. W. Edwards, M. P. Stoykovich, H. H. Solak and P. F. Nealey, *Macromolecules*, 2006, **39**, 3598.
- A. M. Welander, H. Kang, K. O. Stuen, H. H. Solak, M. Müller, J. J. dePablo and P. Nealey, *Macromolecules*, 2008, **41**, 2759.
- R. Ruiz, H. Kang, F. A. Detcheverry, E. Dobisz, D. S. Kercher, T. R. Albrecht, J. J. Pablo and Nealey, P. F. *Science*, 2008, **321**, 936.
- Y. Tada, H. Yoshida, T. Hirai, J. K. Bosworth, E. Dobisz, R. Ruiz, M. Takenaka, T. Hayakawa and H. Hasegawa, *Macromolecules*, 2012, **45**, 292.
- J. G. Son, H. Kang, K. Y. Kim, J. S. Lee, P. F. Nealey and K. Char, *Macromolecules*, 2012, **45**, 150.
- H. Yoshida, H. S. Suh, A. R. Hernandez, J. I. Lee, K. Aida, L. Wan, Y. Ishida, Y. Tada, R. Ruiz, J. J. dePablo and Nealey, *J. Photopolym. Sci Technol.*, 2013, **26**, 55.
- P. A. R. Delgadillo, R. Gronheid, G. Lin, Y. Cao, A. Romo, M. Somervell, K. Nafus and P. F. Nealey, *Proc. Of SPIE*, 8680, 86801H-1.
- S. Xiao, X. M. Yang, S. Park, D. Weller and T. P. Russell, *Adv. Mater.*, 2009, **21**, 2516.
- Y. Tada, H. Yoshida, T. Hirai, J. K. Bosworth, E. Dobisz, R. Ruiz, M. Takenaka, T. Hayakawa and H. Hasegawa, *Macromolecules*, 2012, **45**, 292.
- W. Gu, J. Xu, J. K. Kim, S. W. Hong, X. Wei, X. Yang, K. Y. Lee, D. S. Kuo, S. Xiao and T. P. Russell, *Adv. Mater.*, 2013, **25**, 3677.
- Y. S. LeJung, J. B. Chang, E. Verploegen, K. K. Berggren, C. A. Ross, *Nano Lett.* 2010, **10**, 1000.
- M. Anthamatten and P. T. Hammond, *J. Polym. Sci., Part B: Polym. Phys.*, 2001, **39**, 2671.
- J. Sanger, W. Gronski, S. Maas, B. Heck, *Macromolecules*, 1997, **30**, 6783.
- G. Mao, J. Wang, S. R. Clingman, C. K. Ober, J. T. Chen, E. L. Thomas, *Macromolecules*, 1997, **30**, 2556.
- M. Anthamatten, W. Y. Zheng, P. T. Hammond, *Macromolecules*, 1999, **32**, 4838.
- Y. Tian, K. Watanabe, X. Kong, J. Abe and T. Iyoda, *Macromolecules*, 2002, **35**, 3739.
- K. Watanabe, H. Yoshida, K. Kamata and T. Iyoda, *Trans. Mater. Res. Soc. Jpn.*, 2005, **30**, 377.
- M. Komura and T. Iyoda, *Macromolecules*, 2007, **40**, 4106.
- M. Komura, H. Komiyama, K. Nagai and T. Iyoda, *Macromolecules*, 2013, **46**, 9013.
- H. Komiyama, R. Sakai, S. Hadano, S. Asaoka, K. Kamata, T. Iyoda, M. Komura, T. Yamada and H. Yoshida, *Macromolecules*, 2014, **47**, 1777.
- M. Komura, A. Yoshitake, S. Otake, H. Komiyama and T. Iyoda, T. submitted to *Macromolecules*, 2014.
- J. Li, K. Kamata, S. Watanabe and T. Iyoda, *Adv. Mater.*, 2007, **19**, 1267.
- J. Li, K. Kamata and T. Iyoda, *Thin Solid Films*, 2008, **516**, 2577.
- A. Chen, M. Komura, K. Kamata and T. Iyoda, *Adv. Mater.*, 2008, **20**, 763.
- R. Watanabe, K. Kamata and T. Iyoda, *J. Mater. Chem.*, 2008, **18**, 5482.
- R. Watanabe, T. Iyoda and K. Ito, *Electrochemistry*, 2009, **77**, 214.
- W. Zou, Y. Wang, Z. Wang, A. Zhou, J. Li, A. Chang, Q. Wang, M. Komura, K. Ito and T. Iyoda, *Nanotechnology*, 2011, **22**, 335301.
- S. Asaoka, T. Uekusa, H. Tokimori, M. Komura, T. Iyoda, T. Yamada and H. Yoshida, *Macromolecule*, 2011, **44**, 7645.
- H. Komiyama, T. Iyoda and K. Kamata, *Chem. Lett.*, 2012, **41**, 110.
- T. Goda and T. Iyoda, *J. Mater. Chem.*, 2012, **22**, 9477.
- N. Yamashita, H. Komiyama, Y. Zhao, M. Komura, T. Iyoda and K. Nagai, *Jpn. J. Appl. Phys.*, 2012, **51**, 076704.

- 40 S. Hadano, H. Handa, K.; Nagai, T. Iyoda, J. Z. Li and S. Watanabe, *Chem. Lett.*, 2013, **42**, 7173.
- 41 P. Mansky, Y. Liu, E. Huang, T. P. Russell, C. Hawker, *Science*, 1997, **275**, 1458.
- 42 C. C. Liu, A. R. Hernandez, E. Han, G. S. W. Craig, Y. Tada, H. Yoshida, H. Kang, S. Ji, P. Gopalan, J. J. dePablo and P. F. Nealey, *Macromolecules*, 2013, **46**, 1415.
- 43 M. Husseman, E. E. Malmstrom, M. McNamara, M. Mate, D. Mecerreyes, D. G. Benoit, J. L. Hedric, P. Mansky, E. Huang, T. P. Russell and C. J. Hawker, *Macromolecules*, 1999, **32**, 1424.
- 44 B. Kim, D. Y. Ryu, V. Pryamisyn, V. Ganesan, *Macromolecules*, 2009, **42**, 7917.
- 45 S. Sastry, D. S. Corti, P. G. Debenedetti and F. H. Stillinger, *Phys. Rev. E*, 1997, **56**, 5524.
- 46 Z. Huo, C. Tsung, W. Huang, X. Zhang and P. Yang, *Nano Lett.*, 2008, **8**, 2041.
- 47 T. Miyazaki, R. Hasegawa, H. Yamaguchi, H. Oh-oka, H. Nagato, I. Amemiya and S. Uchikoga, *J. Phys. Chem. C*, 2009, **113**, 8484.

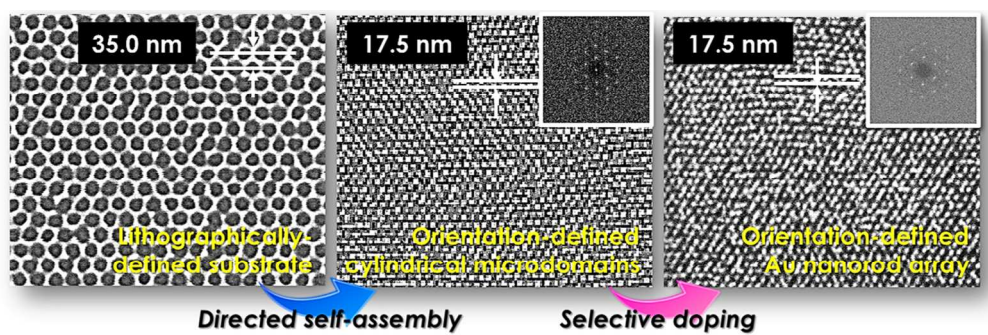


Table of content for this manuscript
236x78mm (150 x 150 DPI)